JCTC Journal of Chemical Theory and Computation

Article

pubs.acs.org/JCTC

Implementation and Application of the Frozen Density Embedding Theory with the Algebraic Diagrammatic Construction Scheme for the Polarization Propagator up to Third Order

Stefan Prager,*,† Alexander Zech,‡ Tomasz A. Wesolowski,‡ and Andreas Dreuw*,†

†Interdisciplinary Center for Scientific Computing, Ruprecht-Karls University, Im Neuenheimer Feld 205A, 69120 Heidelberg, Germany

‡Dèpartement de Chimie Physique, Université de Genève, 30 Quai Ernest-Ansermet, 1211 Genève, Switzerland

Supporting Information

ABSTRACT: Implementation, benchmarking, and representative applications of the new FDE-ADC(3) method for describing environmental effects on excited states as a combination of frozen density embedding (FDE) and the algebraic-diagrammatic construction scheme for the polarization propagator of third order (ADC(3)) are presented. Results of FDE-ADC(3) calculations are validated with respect to supersystem calculations on test systems with varying molecule−environment interaction strengths from dispersion up to multiple hydrogen bonds. The overall deviation compared to the supersystem calculations is as small as 0.029 eV for excitation energies, which is even smaller than the intrinsic error of ADC(3). The dependence of the accuracy on the choice of method and functional for the calculation of the environment and the nonelectrostatic part of the system−environment interaction is evaluated. In three representative examples, the FDE-ADC method is applied to investigate larger systems and to analyze excited state properties using visualization of embedded densities and orbitals.

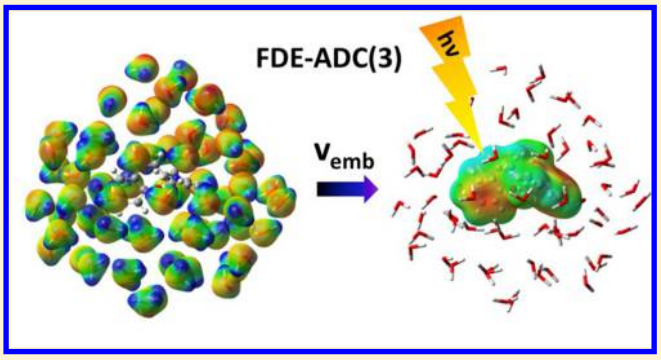

1. INTRODUCTION

Quantum chemical calculations are carried out most easily in the gas phase, but most experimental results are obtained in solution or solid phase. Therefore, including the effects of the environment on chemical and physical properties of the investigated molecule in calculations becomes increasingly important. Electronically excited states in particular are prone to the influence of an environment. Excitation energies can be and usually are shifted, an effect known as solvatochromism.[1] A full supermolecular quantum chemical treatment of a molecule and its environment, however, can easily exceed the limits of feasible calculations due to the high scaling factors of state of the art ab initio methods. Hence, further approximations for including the effects of the environment are required.

Primarily, two different approaches for including the environment in an approximative way have been established: implicit and explicit solvent models. In the former, the environment is usually described as a homogeneously polarizable medium, like in polarizable continuum models (PCM),[2,3] whereas the latter explicitly describes the molecules of an environment. This allows for modeling of specific solute−solvent interactions, for instance, hydrogen bonds, which cannot correctly be described using implicit models.[4,5] An example for explicit solvent interaction is the typical QM/MM approach.[6]

A more recent development in the framework of explicit environment models is represented by density embedding methods.[7−10] In frozen density embedding theory (FDET)[7,11] in particular, the system is divided into two parts: the embedded system (A) and the environment (B). A is then seen as embedded into the electronic density of system B, which is kept unchanged (frozen). Embedded system A can be treated on the DFT level of theory[12−14] but also, as shown in more recent developments, using wave function-based methods.[8,11,15,17,18,41] Furthermore, coupled cluster (CC) in DFT and CC in CC embedding have been established using methods based on FDET.[16,19−22] The density of the environment is usually obtained from lower level quantum chemical calculations,[11] theories for ensembles,[23] or even from experiments. An embedding potential is then created using the environment density ($\rho_B(r)$) as well as the density of the embedded system ($\rho_A(\vec{r})$). In standard form of FDET, herein referred to as conventional FDET, an iterative scheme is needed to create an embedding potential that is self-consistent with the wave function or density of system A.[17,18,24,25]

The FDET variant used in our approach depends on a reference density of A ($(\rho_A^{ref}(\vec{r}))$ and will herein be referred to as

Received: May 4, 2017
Published: September 1, 2017

DOI: 10.1021/acs.jctc.7b00461
J. Chem. Theory Comput. 2017, 13, 4711−4725

linearized FDET.[26,27] This facilitates the use of the same embedding potential for all electronically excited states as it circumvents its state dependence and maintains orthogonality between the states. It can be used in combination with TD-DFT and wave function-based excited state methods, the latter of which lead to more systematic and reliable calculations owing to the known limitations of TD-DFT.[28−30]

In this context, the algebraic diagrammatic construction scheme (ADC) for the polarization propagator in third order is an established and accurate method to calculate electronically excited states.[31,32] Because it is based on perturbation theory and on a noniterative ground state method, the inclusion of external one-particle potentials via the Fock operator is quite straightforward. The ADC(3) method is Hermitian, size-consistent, and systematically improvable.[33] ADC(3) is in particular a very accurate excited state method also capable of describing electronically doubly excited states where ADC(2) has known limitations.[32]

In previous work, we have presented the first combination of FDET and ADC(2).[34] In this article, we briefly review the theory of ADC and FDET in section 2. In section 3 we present the user-friendly implementation of FDE-ADC up to third order perturbation theory (FDE-ADC(3)) in a quantum chemical software package. In section 4, our results are presented, and in subsection 4.1, the best choice of xc-functional for the calculation of the embedding potential is investigated. Subsection 4.2 is denoted to benchmarking of the new FDE-ADC(3) method. In section 5, representative applications of FDE-ADC methods are shown. The paper concludes with a summary of the main results of our work in section 6.

2. THEORETICAL METHODOLOGY

2.1. Algebraic Diagrammatic Construction Scheme for the Polarization Propagator. The algebraic diagrammatic construction scheme for the polarization propagator (ADC) is a size-extensive and Hermitian method for calculation of vertically excited correlated electronic states. It is based on the Møller−Plesset partitioning of the Hamilton operator and can therefore be seen as "perturbation theory for excited states". A full derivation of ADC is given in the literature.[35−39] As shown previously,[33] ADC can be derived using the intermediate state (IS) formalism. In this representation, the ADC matrix is given as the Hamilton operator shifted by the ground state energy E_0

$$M_{IJ} = \langle \tilde{\Psi}_I | \hat{H} - E_0 | \tilde{\Psi}_J \rangle \tag{1}$$

which leads to a Hermitian eigenvalue problem

$$\mathbf{MX} = \mathbf{X\Omega},\ \mathbf{X}^{\dagger}\mathbf{X} = \mathbf{1} \tag{2}$$

with $\mathbf{X}$ as the matrix of eigenvectors corresponding to the excited states, and Ω as the matrix of eigenvalues corresponding to the excitation energies. In general, the order of perturbation theory used for the construction of the intermediate state representation (ISR) determines the order of the ADC scheme. Using second order perturbation theory (MP(2)) in the IS formalism results in second order ADC equations (ADC(2)), and using third order perturbation theory (MP(3)) yields third order ADC equations (ADC(3)).[32,33,35,38,39]

2.2. Frozen Density Embedding Theory (FDET) and Linearized FDET. FDET has been previously derived in the literature;[11,26] however, for completeness, a brief introduction is given in this section. In FDET, the supersystem is divided into the embedded system (A) and the environment (B). The density of the environment, once obtained, is kept frozen through the whole calculation. An embedding potential $v_{\mathrm{emb}}(\vec{r})$ is created from the densities of both subsystems. This potential is used as an external potential for the embedded system A, i.e., A is embedded in the density of B. Because FDET exhibits similarities to QM/MM approaches, it shares its limitations. One cannot easily break covalent bonds when dividing a supersystem into the two fragments. Electronic processes including both fragments, like charge-transfer excitation from fragment A to B, are difficult to model. Hence, standard FDET is only applicable for systems amenable for QM/MM-type of embedding methods. For describing electronic processes on both fragments like coupled excitations, special variants of FDET are needed.[40]

In this work, A is treated using ADC(3) instead of DFT, whereas the density of B can be computed using either wave function- or density-based methods. Thus, the FDET total energy of the supersystem is given as[27]

$$E_{\mathrm{AB}}^{\mathrm{EWF}}[\Psi_{\mathrm{A}}, \rho_{\mathrm{B}}] = \langle \Psi_{\mathrm{A}} | \hat{H}_{\mathrm{A}} | \Psi_{\mathrm{A}} \rangle + V_{\mathrm{B}}^{\mathrm{nuc}}[\rho_{\mathrm{A}}] + J_{\mathrm{int}}[\rho_{\mathrm{A}}, \rho_{\mathrm{B}}] + E_{\mathrm{xc},T}^{\mathrm{nad}}[\rho_{\mathrm{A}}, \rho_{\mathrm{B}}] + E_{v_{\mathrm{B}}}^{\mathrm{HK}}[\rho_{\mathrm{B}}] + V_{\mathrm{A}}^{\mathrm{nuc}}[\rho_{\mathrm{B}}] \tag{3}$$

with

$$J_{\mathrm{int}}[\rho_{\mathrm{A}}, \rho_{\mathrm{B}}] = \int\int \frac{\rho_{\mathrm{A}}(\vec{r})\rho_{\mathrm{B}}(\vec{r}')}{|\vec{r} - \vec{r}'|}\, \mathrm{d}\vec{r}\ \mathrm{d}\vec{r}' \tag{4}$$

$$V_{\mathrm{A}}^{\mathrm{nuc}}[\rho_{\mathrm{B}}] = \int \rho_{\mathrm{B}}(\vec{r}) v_{\mathrm{A}}(\vec{r})\, \mathrm{d}\vec{r} \tag{5}$$

$$V_{\mathrm{B}}^{\mathrm{nuc}}[\rho_{\mathrm{A}}] = \int \rho_{\mathrm{A}}(\vec{r}) v_{\mathrm{B}}(\vec{r})\, \mathrm{d}\vec{r} \tag{6}$$

$$E_{\mathrm{xc},T}^{\mathrm{nad}}[\rho_{\mathrm{A}}, \rho_{\mathrm{B}}] = E_{\mathrm{xc}}^{\mathrm{nad}}[\rho_{\mathrm{A}}, \rho_{\mathrm{B}}] + T_{\mathrm{s}}^{\mathrm{nad}}[\rho_{\mathrm{A}}, \rho_{\mathrm{B}}] + \Delta F^{\mathrm{MD}}[\rho_{\mathrm{A}}] \tag{7}$$

These terms describe the interaction between the embedded species A and the environment B. $J_{\mathrm{int}}[\rho_{\mathrm{A}}, \rho_{\mathrm{B}}]$, $V_{\mathrm{A}}^{\mathrm{nuc}}[\rho_{\mathrm{B}}]$ and $V_{\mathrm{B}}^{\mathrm{nuc}}[\rho_{\mathrm{A}}]$ correspond to Coulombic electron−electron repulsion, attraction between electron density of B with nuclei of A, and attraction between electron density of A with nuclei of B, respectively. $E_{\mathrm{xc},T}^{\mathrm{nad}}[\rho_{\mathrm{A}},\rho_{\mathrm{B}}]$ describes a nonadditive energy bifunctional and comprises terms for exchange-, correlation-, and kinetic density functionals. Typically, the ρ_{A}-dependent functional $\Delta F^{\mathrm{MD}}[\rho_{\mathrm{A}}]$ is neglected in practice because its contributions are usually small.[41] It corresponds to the difference in describing the embedded system as a real interacting many-electron system or as a reference system of noninteracting electrons. In the total energy formulation, the term $E_{v_{\mathrm{B}}}^{\mathrm{HK}}[\rho_{\mathrm{B}}]$ refers to the energy of the isolated subsystem B calculated at the Hohenberg−Kohn DFT level of theory. The nonadditive energy bifunctional is defined as

$$E^{\mathrm{nad}}[\rho_{\mathrm{A}}, \rho_{\mathrm{B}}] = E[\rho_{\mathrm{A}} + \rho_{\mathrm{B}}] - (E[\rho_{\mathrm{A}}] + E[\rho_{\mathrm{B}}]) \tag{8}$$

Building the functional derivative of the total energy expression (eq 3) with respect to the electron density of A (ρ_{A}), one obtains the embedding potential $v_{\mathrm{emb}}(\vec{r})$, which reads

$$v_{\mathrm{emb}}[\rho_{\mathrm{A}}, \rho_{\mathrm{B}}, v_{\mathrm{B}}](\vec{r}) = v_{\mathrm{B}}(\vec{r}) + \int \frac{\rho_{\mathrm{B}}(\vec{r}')}{|\vec{r} - \vec{r}'|}\, \mathrm{d}\vec{r}' + \frac{\delta E_{\mathrm{xc},T}^{\mathrm{nad}}[\rho_{\mathrm{A}}, \rho_{\mathrm{B}}]}{\delta \rho_{\mathrm{A}}(\vec{r})} \tag{9}$$

Because the embedding potential, which is used to compute the electron density of system A, depends itself on the density of system A, the resulting equation is nonlinear and has to be solved

DOI: 10.1021/acs.jctc.7b00461
J. Chem. Theory Comput. 2017, 13, 4711−4725

iteratively. In the further approximated version of FDET, denoted as linearized FDET, the electron density of A (ρ_A) in the embedding potential is replaced by the constant ground state reference density ρ_A^{ref}. In linearized FDET, the functional $E_{xc,T}^{nad}[\rho_A\rho_B]$ is approximated by means of the truncated Taylor series about some reference density $\rho_A^{ref}(\vec{r})$. Higher than linear terms are neglected.

$$E_{xc,T}^{nad}[\rho_A, \rho_B] \approx E_{xc,T}^{nad}[\rho_A^{ref}, \rho_B] + \int (\rho_A(\vec{r}) - \rho_A^{ref}(\vec{r})) \frac{\delta E_{xc,T}^{nad}[\rho_A^{ref}, \rho_B]}{\delta \rho_A^{ref}(\vec{r})} d\vec{r} = E_{xc,T}^{nad}[\rho_A^{ref}, \rho_B] + \Delta^{lin}[\rho_A, \rho_A^{ref}, \rho_B] \quad (10)$$

Then, the total energy expression in linearized FDET is now linear in ρ_A and reads

$$\begin{aligned} E_{AB}^{linFDET}[\Psi_A, \rho_B, \rho_A^{ref}] &= \langle \Psi_A | \hat{H}_A | \Psi_A \rangle + \int \rho_A(\vec{r}) v_B(\vec{r}) d\vec{r} + \int \rho_B(\vec{r}) v_A(\vec{r}) d\vec{r} \\ &+ \iint \frac{\rho_A(\vec{r}) \rho_B(\vec{r}')}{|\vec{r} - \vec{r}'|} d\vec{r} d\vec{r}' + E_{xc}^{nad}[\rho_A^{ref}, \rho_B] \\ &+ T_s^{nad}[\rho_A^{ref}, \rho_B] + E_{v_B}^{HK}[\rho_B] + \Delta^{lin}[\rho_A, \rho_A^{ref}, \rho_B] \end{aligned} \quad (11)$$

The corresponding embedding potential is independent of the electronic state of the embedded system A and is given as

$$v_{emb}[\rho_A^{ref}, \rho_B, v_B](\vec{r}) = v_B(\vec{r}) + \int \frac{\rho_B(\vec{r}')}{|\vec{r} - \vec{r}'|} d\vec{r}' + \frac{\delta E_{xc,T}^{nad}[\rho_A^{ref}, \rho_B]}{\delta \rho_A^{ref}} \quad (12)$$

Note that eq 11 for energy and eq 12 for potential are self-consistent. The embedding potential is a functional derivative of the corresponding contribution to the total energy. This embedding potential will from here on be denoted as $v_{emb}^{lin}(\vec{r})$. It is added to the ground state Hamiltonian, resulting in the following Schrödinger-like equation

$$(\hat{H}_A + \hat{v}_{emb}^{lin})\Psi_A = \epsilon \Psi_A \quad (13)$$

In the evaluation of the expectation value of the Hamiltonian, the expectation value of the embedding potential is also calculated, which includes all electrostatic and part of the nonelectrostatic terms.

$$\langle \Psi_A | \hat{v}_{emb}^{lin} | \Psi_A \rangle = V_B^{nuc}[\rho_A] + J_{int}[\rho_A, \rho_B] + \int \rho_A(\vec{r}) \frac{\delta E_{xc,T}^{nad}[\rho_A^{ref}, \rho_B]}{\delta \rho_A^{ref}(\vec{r})} d\vec{r} \quad (14)$$

Thus, for the evaluation of the total energy expression, eq 11 can be rewritten as

$$\begin{aligned} E_{AB}^{linFDET}[\Psi_A, \rho_B, \rho_A^{ref}] &= \langle \Psi_A | \hat{H}_A + \hat{v}_{emb}^{lin}(\vec{r}) | \Psi_A \rangle + \int \rho_B(\vec{r}) v_A(\vec{r}) d\vec{r} + \Delta F^{MD}[\rho_A^{ref}] \\ &+ E_{v_B}^{HK}[\rho_B] + E_{xc,T}^{nad}[\rho_A^{ref}, \rho_B] - \int \rho_A^{ref}(\vec{r}) \frac{\delta E_{xc,T}^{nad}[\rho_A^{ref}, \rho_B]}{\delta \rho_A^{ref}(\vec{r})} d\vec{r} \end{aligned} \quad (15)$$

Hence, after evaluation of the Hamiltonian including the embedding potential, only constant, state-independent terms have to be added. Thus, the excitation energy, which is defined as the energy difference between different states, simplifies to

$$\Delta E_{IJ} = \langle \Psi_A^J | \hat{H}_A + \hat{v}_{emb}^{lin} | \Psi_A^J \rangle - \langle \Psi_A^I | \hat{H}_A + \hat{v}_{emb}^{lin} | \Psi_A^I \rangle \quad (16)$$

because all other terms cancel exactly.

3. IMPLEMENTATION AND COMPUTATIONAL METHODOLOGY

Continuing our previous work,[34] the FDE-ADC algorithm has been implemented as a module called `FDEman` into the quantum chemical program package Q-Chem.[42] In this article, we present for the first time an implementation of FDE-ADC up to third order for both core and valence excitations, i.e., FDE-ADC(3) and FDE-CVS-ADC(3).

The procedure of an FDE-ADC calculation comprises four steps: (a) generation of ρ_A, (b) generation of ρ_B, (c) calculation of $v_{emb}^{lin}(\vec{r})$, and finally (d) applying $v_{emb}^{lin}(\vec{r})$ in an FDE-ADC calculation. In the first step, fragment A is initialized. and a density matrix in the basis of atomic orbitals at the corresponding level of Møller−Plesset perturbation theory[43,44](MP) is computed employing the `adcman`[31] module in Q-Chem. This density matrix (ρ_A^{ref}) is stored; in the next step, the environment fragment B is initialized, and either a Hartree−Fock (HF)[45] or a density-functional theory (DFT)[12−14] calculation can be performed to obtain the density matrix ρ_B. In a third step, the two density matrices of A and B are used to evaluate the four state-independent parts of the embedding potential, which are the nuclear attraction potential, the Coulombic repulsion potential, and the exchange-correlation and kinetic energy nonadditive bifunctional potentials (see eq 12). The expectation value as well as the derivative of the nonadditive functionals are calculated using integration on a standard quadrature grid SG-1.[46] In the last step, an FDE-ADC calculation is performed using the `adcman` module. For this purpose, system A is initialized again, and the previously generated embedding potential is subsequently added to the Fock-Matrix **F** in the SCF procedure of the underlying HF calculation.

$$\tilde{\mathbf{F}} = \mathbf{F} + \hat{v}_{emb}^{lin} \quad (17)$$

Because the influence of the environment is included in the modified orbitals and orbital energies, no changes have to be made to the ADC equations; thus, it is immediately available for all variants of ADC and core−valence separated ADC (CVS-ADC) up to third order.[31,32,47−50] Note that, currently, the algebraic expressions for the ISR in third order are not yet implemented. Therefore, the density matrices are obtained using the ADC vectors at third order with the ISR at second order. Hence, the embedding potential for FDE-ADC(3) is calculated using the MP(2) density for ρ_A^{ref}. Using this approach, it is also possible to employ other features of ADC, e.g., the wave function and density analysis utility `libwfa`,[51−53] or the calculation of spin−orbit coupling elements,[54] which are also implemented in Q-Chem. With these tools, the direct influence of an environment on the excitations of the embedded system can be visualized via difference and transition density analysis, attachment and detachment density plots, or generation of excited state natural orbitals.[50,52]

In general, the only approximations made in FDE-ADC besides the intrinsic approximations in the underlying theories of ADC and DFT are keeping the environment density frozen and using the linearized approach for FDET.

Currently, two different approaches are implemented to perform an FDE-ADC calculation: supermolecular expansion (SE) and reassembling of density matrix (RADM) approaches.

DOI: 10.1021/acs.jctc.7b00461
J. Chem. Theory Comput. 2017, 13, 4711−4725

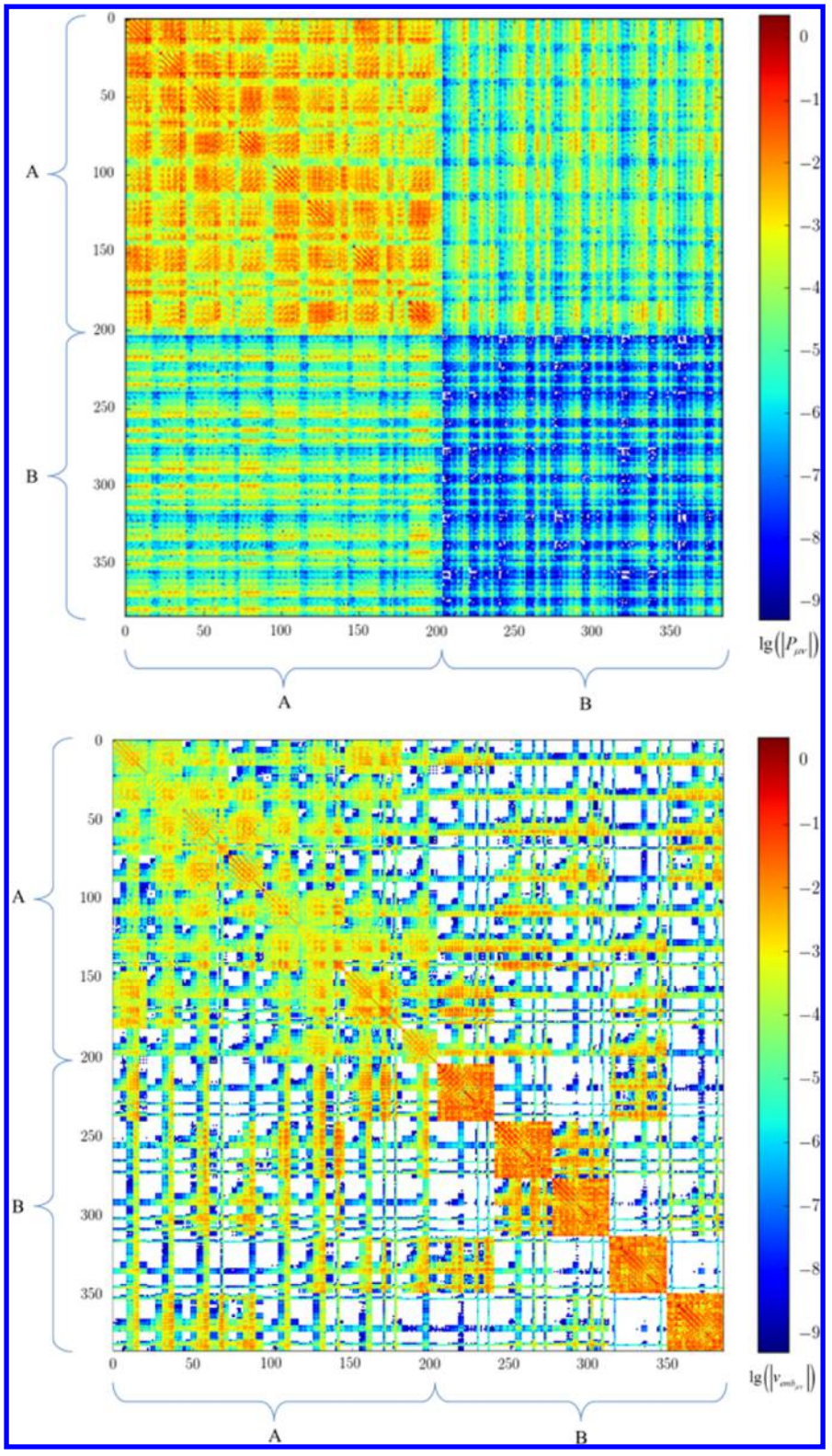

Figure 1. Graphical representation of the values of the reassembled density matrix (top) and the total embedding potential (bottom) of the example system uracil (A) and five water molecules (B) in the basis of both subsystems (A + B). For better visibility, the decadal logarithm of the values is shown. Values below 10^{-10} are treated as zero and displayed as white in the diagram. The maximum density matrix and maximum potential matrix elements are 2.2762 and 0.6346, respectively.

Although the first variant is useful only for benchmark calculations, because it provides no computational savings compared to a supersystem calculation, the second variant can be used for production calculations as shown in section 5.

The RADM approach is an approximation to SE.[34] Using RADM, system A is calculated twice; the first is in the supermolecular basis A + B on the HF level of theory obtaining the HF density matrix. This density matrix contains four blocks:

DOI: 10.1021/acs.jctc.7b00461
J. Chem. Theory Comput. 2017, 13, 4711−4725

AA, AB, BA, and BB. After this, it is calculated again, now in the basis of A only on the MP(2) level of theory, and a separate HF-to-MP(2) difference density matrix in the basis of A is generated. The HF-to-MP(2) difference density matrix is in a following step added to the AA block of the HF density matrix of the previous calculation building a density matrix in the basis of A + B on the MP(2) level of theory in the AA block and on the HF level of theory on the remaining AB, BA, and BB blocks, which is called the reassembled density matrix. The environment system B is, as in SE, calculated in the supermolecular basis A + B. The subsequent calculation of the embedding potential is performed in the supermolecular basis as well. However, after the embedding potential is complete, it is truncated to the AA block only. This approximation is valid because, in the supermolecular basis, the values of the embedding potential in the off-diagonal AB and BA blocks and the values of the density matrix of A in the BB block are almost zero (see Figure 1). Hence, in a contraction of the density matrix of A with the embedding potential, the values in these three blocks vanish and can therefore be neglected. Consequently, the FDE-ADC calculation (step d), which is the computationally most demanding step, can be performed in the basis of A only. In summary, the RADM approximation consists of an assembling of a density matrix and the truncation of the calculated embedding potential. Benchmark calculations have shown that the errors of the FDE-ADC method in general and the error of the RADM approximation in particular are lower than the intrinsic error of the ADC method used.[34]

For the FDE-ADC calculations, a development version of Q-Chem based on version 4.4 has been used. This implementation of FDE-ADC in the module `FDEman` will be available in one of the upcoming releases of Q-Chem. Molecular pictures were captured using Avogadro 1.1.0.,[55] POV-Ray 3.7.0.RC6,[56] Jmol 13.0.14,[57] and GaussView 5.0.8[58]

4. BENCHMARKING AND TESTING

4.1. Influence of the Method and Functional on the Embedding Potential. In this section, various methods for the calculation of the environment (fragment B) and the generation of the density ρ_B are tested. For this comparison, three representative model systems were used. The first model system consists of a benzene molecule as system A and a hydrogen fluoride (HF) molecule placed side-on and almost in-plane with the benzene ring as the environment ([BZ·HF]). As the second model system, a benzaldehyde molecule was used as the embedded system, and two water molecules forming a dimer and building a hydrogen bond to the oxygen atom of the benzaldehyde were used as the environment ([BA·2H_2O]). The last model system consists of a uracil molecule for A and five water molecules as B ([UC·5H_2O]). The water molecules exhibit various hydrogen bonds both among themselves and to the uracil molecule. This set of systems accounts for various interaction strengths between the embedded system and environment as well as different kinds of excited states. Athough the first system (benzene and HF) shows only weak and polarization-based interactions, the benzaldehyde is more influenced by the environment due to the hydrogen bond in addition to the polarization of the π-system. The uracil system shows intense interactions between the core system and the environment including various hydrogen bonds. All three benchmark systems are shown in Figure 2.

The excited states of all three systems for the supersystem, the core system alone, and in the FDE-ADC(2) approach have been

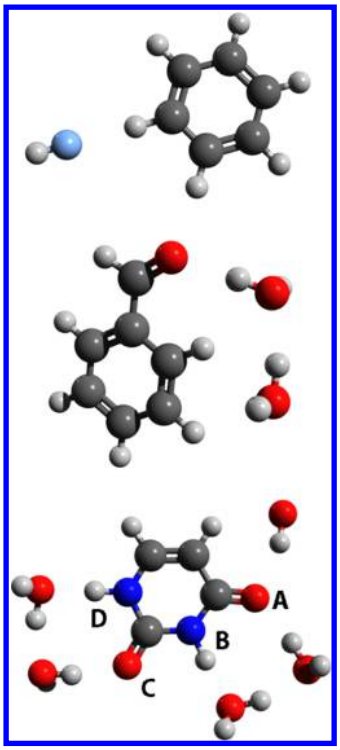

Figure 2. Molecular structures of the three test systems: benzene with a hydrogen fluoride ([BZ·HF]) (top), benzaldehyde with two water molecules ([BA·2H_2O])(middle), and uracil with five water molecules ([UC·5H_2O]) (bottom).

studied in great detail previously.[34] For all investigations, the supersystem is optimized at the MP(2)/cc-pVDZ level of theory. This ensures that no geometrical changes influence the comparison between the FDE approach and the supersystem calculation. Because the influence of the computational method, essentially the choice of xc-functional, for the environment is here in the focus of the investigation, it suffices to perform the final FDE-ADC calculation only at the second-order of perturbation theory.

A large set of methods used to calculate the environment was chosen including HF, generalized gradient approximation (GGA)-DFT (BLYP,[59,60] PBE,[61] BP86,[59,62] and PW91[63]) and hybrid-DFT functionals (B3LYP,[64] BHLYP,[59,60] B5050LYP,[65] PBE0,[66] and SOGGA11-X[67]). For the evaluation of the nonadditive bifunctional in the embedding potential, only explicit density functionals are considered. Hence, the following GGA-DFT functionals were used to approximate the non-additive exchange-correlation contribution to the energy and potential: PBE,[61] BLYP,[59,60] BP86,[59,62] $G96_{corr}$[68]-$P86_{ex}$,[62] GAM,[69] PW91,[63] and SOGGA11.[70] In all calculations, the Thomas−Fermi kinetic energy functional[71] was used for the kinetic energy contribution to the FDET energy and embedding potential. For all calculations, the basis set cc-pVDZ[72] was used.

For all systems, the lowest five electronically excited states of the supersystem were calculated as reference at the ADC(2)/cc-pVDZ level of theory. For comparison, RADM-FDE-ADC(2)/cc-pVDZ calculations were performed employing all possible combinations of the aforementioned methods for the calculation of the environment with xc-functionals for the calculation of the embedding potential. Because in all cases the supersystem calculation serves as reference, deviations in excitation energies are given relative to the supersystem. Therefore, negative

DOI: 10.1021/acs.jctc.7b00461
J. Chem. Theory Comput. 2017, 13, 4711−4725

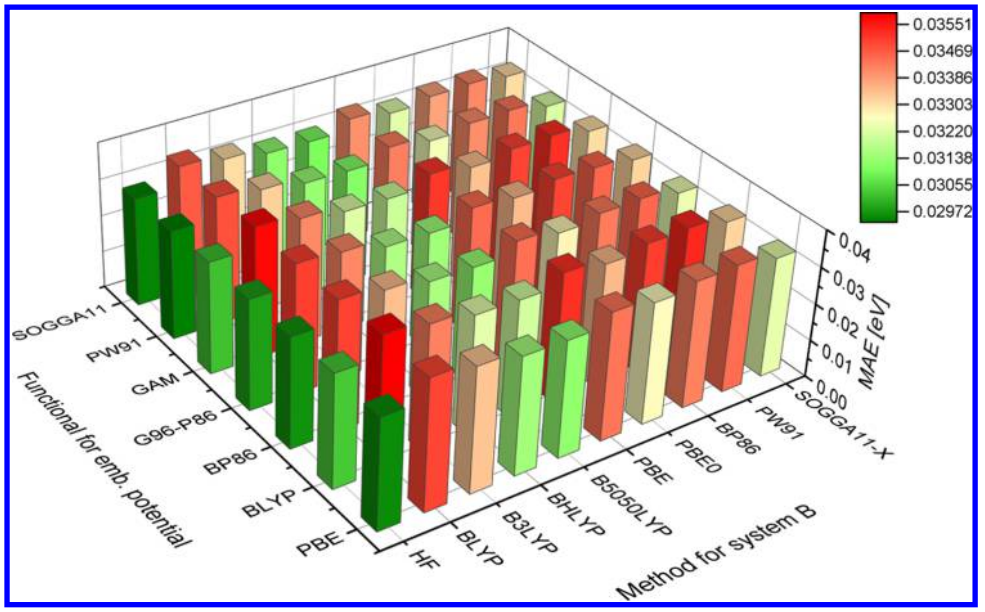

Figure 3. Mean absolute errors (MAE) of the environment induced excitation energy shifts of the computed states of all three investigated systems (benzene + hydrogen fluoride, benzaldehyde + two water molecules, and uracil + five water molecules) for all investigated combinations of methods to calculate the environment density and the functional to calculate the nonelectrostatic part of the embedding potential.

deviations of the excitation energy correspond to higher excitation energies in the supersystem than in the embedded system.

Because the investigation of the dependence of the FDE-ADC results on the choice of ρ_B and on the approximations for exchange-correlation functional is more or less only a side-aspect of this paper, only the conclusion is given here. Detailed analyses and the data supporting these conclusions are available in the Supporting Information.

To summarize the key results, the test of three different systems with environment interactions ranging from weak polarization up to multiple hydrogen bonds shows only marginal dependence of the accuracy on the choice of functional used to calculate $v_{emb}^{lin}(\vec{r})$. Despite the very small differences in the MAEs, some functionals can be identified to generally perform better than others in combination with ADC. The most accurate functionals used for the embedding potentials are the PBE and PW91 functionals. The least accurate ones are the BLYP and GAM functionals. A detailed analysis of all our data is given in the Supporting Information. However, overall the differences are tiny and probably not relevant in practical calculations.

Regarding the theoretical method used to calculate the environment density ρ_B, the differences in accuracy are more significant. In general, hybrid functionals and HF itself perform better than functionals without exact exchange. This tendency becomes particularly visible when strong interactions between the embedded system and the environment play a role. In these cases, the accuracy clearly depends on the amount of HF exchange with the more the better. Additionally, it seems not advantageous to apply the same xc-functional for the calculation of ρ_B and for the embedding potential. In fact, it turns out HF has the smallest MAE when ADC is used for the embedded system. The MAEs for all investigated combinations of methods to calculate ρ_B and the xc-functional used in the embedding potential are summarized in Figure 3. A possible explanation for the observed trend is that the density of the embedded system, which is calculated using the MP(2) level of theory, is also largely based on HF theory. This is also the case in the supermolecular reference calculation. Hence, both densities "match" best when both are calculated using the same underlying theoretical model, i.e., HF, as in the supermolecular approach.

4.2. Benchmark of FDE-ADC(3). In this chapter, the first results for the combination of frozen density embedding (FDE) with the algebraic-diagrammatic construction scheme of the polarization propagator of third order (ADC(3)) are presented. Analogously to the previously demonstrated variant FDE-ADC(2),[34] this new method is referred to as FDE-ADC(3). According to the benchmark of FDE-ADC(2), the same test set of (1) [BZ·HF], (2) [BA·2H_2O], and (3) [UC·5H_2O] will be employed (Figure 2). As before, the geometries have been optimized at the MP(2)/cc-pVDZ level of theory for the supersystem and used for all calculations to exclude energy differences due to geometry differences. The supersystems and the isolated core systems (A) were investigated at the ADC(3)/6-311++G**[73−75] level of theory. For the FDE-ADC(3) calculations, the reassembling of density matrix approximation (RADM) and the same basis set 6-311++G** was used because previous studies showed an improved accuracy for FDE-ADC when diffuse basis sets were employed.[34] Only in [BA·2H_2O] was the aug-cc-pVDZ basis set chosen due to convergence issues in the supersystem calculation using the 6-311++G** basis set. The RADM approach was chosen because this is the variant capable of performing productive calculations of larger systems. The HF method was chosen for the calculation of the environment density ρ_B and the PBE functional for the nonelectrostatic part of the embedding potential because this combination exhibits the smallest error as shown in section 4.1.

Note that the supersystem calculation is always taken as reference for both isolated and FDE-ADC(3) results. Hence, solvatochromic shifts and deviations of FDE-ADC from the supersystem results are calculated as $\omega_{isol} - \omega_{sup}$ and $\omega_{FDE\text{-}ADC} - \omega_{sup}$, respectively. As a consequence, a negative value indicates a larger excitation energy in the supersystem (blue shift). The same holds for oscillator strengths.

4.2.1. Benzene and Hydrogen Fluoride. Starting again with the weakly interacting system [BZ·HF], at first, [BZ·HF] and

DOI: 10.1021/acs.jctc.7b00461
J. Chem. Theory Comput. 2017, 13, 4711−4725

Table 1. Excitation Energies, Oscillator Strengths, And Orbital Transitions for the Four Energetically Lowest Electronically Excited Singlet States of Isolated Benzene, [BZ·HF], Using the Supermolecular ADC(3) and FDE-ADC(3) Methods Given >10% Orbital Transitions

	excitation energies [eV] and osc. str.			orb. trans.	weight [%]		
state	iso.[a]	sup.[b]	FDE[c]	H + x → L + y[d]	iso.[a]	sup.[b]	FDE[c]
S_1	5.049 (0.0000)	5.050 (0.0001)	5.049 (0.0001)	0 → 6 ($\pi \rightarrow \pi^*$)	36.8	37.5[e]	37.5
				−1 → 7 ($\pi \rightarrow \pi^*$)	36.8	34.8[e]	35.4
S_2	6.369 (0.0000)	6.292 (0.0008)	6.293 (0.0007)	0 → 0 ($\pi \rightarrow R$)	79.2	18.0	27.3
				0 → 1 ($\pi \rightarrow R$)		57.8	51.9
S_3	6.369 (0.0000)	6.310 (0.0000)	6.312 (0.0000)	−1 → 0 ($\pi \rightarrow R$)	79.2	18.0	27.5
				−1 → 1 ($\pi \rightarrow R$)		56.1	50.4
S_4	6.405 (0.0000)	6.396 (0.0000)	6.397 (0.0001)	−1 → 6 ($\pi \rightarrow \pi^*$)	42.1	42.0[e]	42.1
				0 → 7 ($\pi \rightarrow \pi^*$)	42.1	40.7[e]	41.5

[a]Isolated benzene. [b]Supermolecular ADC(3). [c]RADM-FDE-ADC(3). [d]H = HOMO, L = LUMO, R = Rydberg-type orbital. [e]An orbital localized at the hydrogen fluoride is neglected in counting (see text).

isolated benzene are investigated. Next, an FDE-ADC(3) calculation is performed, and the results are compared to the supermolecular calculations. Although the occupied frontier orbitals, i.e., the highest occupied molecular orbital (HOMO) and HOMO−1 are typical π orbitals, the corresponding unoccupied frontier orbitals, i.e., the lowest unoccupied molecular orbital (LUMO) and LUMO+1, are not necessarily the corresponding π^* orbitals. Because of the diffuse basis functions, Rydberg and various other types of virtual orbitals are present compared to calculations using basis sets without diffuse basis functions. Therefore, the corresponding π^* to the HOMO and HOMO−1 are LUMO+7 and LUMO+8 in the supermolecular calculation. The LUMO+1, for example, is a Rydberg orbital (R) located in the benzene ring plane opposite the hydrogen fluoride.

The four energetically lowest electronically excited states of [BZ·HF] were calculated. The S_1 and S_4 states are ($\pi \rightarrow \pi^*$) transitions, whereas S_2 and S_3 are Rydberg states. A detailed analysis of the excitations is given in Table 1. In isolated benzene, HOMO and HOMO−1 have π character, whereas LUMO and LUMO−1 instead are Rydberg orbitals. The energetically lowest π^* orbitals are LUMO+6 and LUMO+7. For isolated benzene, the lowest four excitations were also calculated. The S_1 and S_4 states show ($\pi \rightarrow \pi^*$) character, and the S_2 and S_3 states are Rydberg states. A more detailed analysis is given in Table 1. However, it is noticeable, that in the calculations employing ADC(3)/6-311++G** the solvatochromic shifts differ from the calculations at the ADC(2)/cc-pVDZ level. While using the latter, a solvatrochromic blue shift due to hydrogen fluoride could be observed for states S_1 to S_4 (($\pi \rightarrow \pi^*$) transitions),[34] two ($\pi \rightarrow \pi^*$) excited states show a small red shift at the ADC(3)/6-311++G** level of theory. The deviations to the former calculations at the ADC(2)/cc-pVDZ level are caused by the 6-311++G** basis set. This has been verified by comparison to supermolecular results at the ADC(3)/cc-pVDZ level of theory.

In the RADM-FDE-ADC(3) calculation, the hydrogen fluoride is modeled by virtue of the embedding potential. The resulting orbitals look qualitatively identical to the ones obtained in the isolated benzene calculation. However, because the orbitals localized at the benzene also did not show any difference to the isolated benzene orbitals in the supermolecular calculations, this result is not unexpected. In the supermolecular calculation, additional orbitals located at hydrogen fluoride are included, which are by setup not included in the other calculations. For ease of comparison, this is taken care of in the orbital numbering, and the orbital numbering of the supermolecular calculation is generally adapted.

Overall, the FDE-ADC(3) calculation almost shows quantitative agreement with the supermolecular calculation. The S_1 and S_4 state exhibit ($\pi \rightarrow \pi^*$) transition character, and the S_2 and S_3 states are identified as Rydberg states (Table 1). A diagrammatic representation of the absorbance shift induced by the environment, i.e., the difference between supermolecular calculation and isolated benzene as well as an illustration of the accuracy of the FDE-ADC(3) method in comparison with the supermolecular calculation, is given in Figure 4.

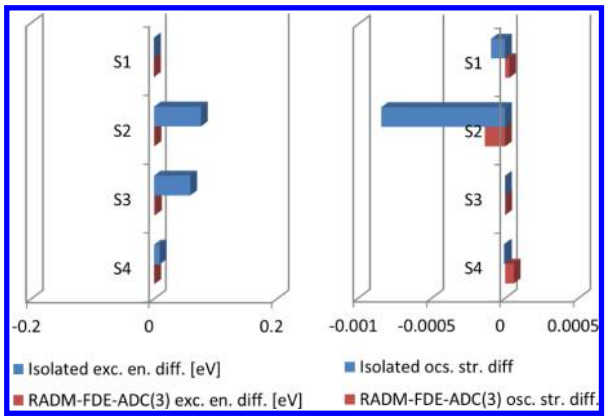

Figure 4. Analysis of the accuracy of FDE-ADC(3) for [BZ·HF]. Excitation energy difference (left) and oscillator strength difference (right) of the isolated benzene to the supersystem (blue) and the FDE-ADC(3) calculation using the RADM approximation to the supersystem (red). The blue bars correspond to the absorbance shift due to the influence of the environment on the excitation energies and oscillator strengths (solvatochromic shift), and the red bars indicate the accuracy of the FDE-ADC(3) calculation in comparison with the ADC(3) supersystem calculation.

The largest deviation in excitation energies is smaller than 0.002 eV and approximately 0.0001 for oscillator strengths when the FDE-ADC(3) calculation is compared to the supermolecular ADC(3) calculation. The mean absolute error (MAE) of all four states in excitation energies is 0.001 eV and 0.0001 for oscillator strengths, respectively.

4.2.2. Benzaldehyde with Two Water Molecules. Analogously to the previous system, FDE-ADC(3) has been tested for [BA·2H_2O]. In both the supermolecular and the isolated benzaldehyde calculations, the HOMO, HOMO−1 and

DOI: 10.1021/acs.jctc.7b00461
J. Chem. Theory Comput. 2017, 13, 4711−4725

HOMO−2 exhibit π, π, and n character, respectively. However, because of the chosen diffuse basis set, corresponding π^* orbitals can be found as LUMO+3 in $[BA{\cdot}2H_2O]$ and LUMO+4 in the isolated benzaldehyde calculation. Obviously, some orbitals changed their energetic order due to the effect of the two water molecules. Further, important π^* orbitals arise as LUMO+7 and LUMO+8 in isolated benzene and as LUMO+9 in $[BA{\cdot}2H_2O]$. The occupied orbitals HOMO and HOMO−1 are reoriented when including the water molecules (see Figure 5).

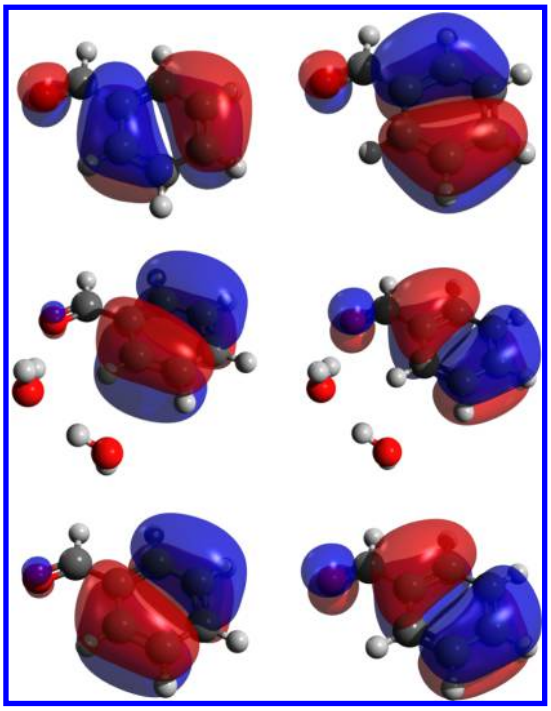

Figure 5. HOMO (left side) and HOMO−1 (right side) of isolated benzaldehyde (top) of $[BA{\cdot}2H_2O]$ calculated with supermolecular ADC(3) (middle) and with FDE-ADC(3) (bottom).

The five energetically lowest excited states have been calculated both for $[BA{\cdot}2H_2O]$ and isolated benzaldehyde. However, in none of these systems and independent from the chosen basis set, the calculations of the fourth excited state (S_4) did converge. In both cases, the first excited state exhibits ($n \rightarrow \pi^*$) excitation character, whereas the states S_2, S_3, and S_5 exhibit local ($\pi \rightarrow \pi^*$) transition character. The solvatochromic shift for benzaldehyde is −0.24 eV for the ($n \rightarrow \pi^*$) excitation and between 0.1 and 0.18 eV for the ($\pi \rightarrow \pi^*$) excitations. A detailed overview of the calculated excited states is given in Table 2. The reorientation of the HOMO and HOMO−1 prevents a direct mapping of the corresponding transitions between isolated benzaldehyde and the supermolecular calculation. However, because the orbitals are still of the same type and form and the orbital energies are also quite similar, this change does not affect the character of the excited states themselves.

In the FDE-ADC(3) calculations, the influence of the environment is very well reproduced. Furthermore, the reorientation of the HOMO and HOMO−1 is reproduced in the FDE-ADC(3) calculations (Figure 5). The MAE in excitation energies is 0.031 eV and in oscillator strength is 0.0092. The character of the excited states, compared to $[BA{\cdot}2H_2O]$, is retained. Whereas S_1 has an ($n \rightarrow \pi^*$) character, S_2, S_3, and S_5 states exhibit ($\pi \rightarrow \pi^*$) character. A diagrammatic representation of the accuracy of the FDE-ADC(3) calculation for $[BA{\cdot}2H_2O]$ is given in Figure 6.

4.2.3. Uracil with Five Water Molecules. For the last benchmark system, $[UC{\cdot}5H_2O]$, the same analysis has been performed. HOMO and HOMO−1 in both the $[UC{\cdot}5H_2O]$ and the isolated uracil exhibit π character. HOMO−2 and HOMO−3 are n orbitals localized at the oxygen atoms. Calculation of the five energetically lowest excited states of $[UC{\cdot}5H_2O]$ reveals four ($\pi \rightarrow \pi^*$) transitions, i.e., S_1, S_3, S_4, and S_5. The S_2 state exhibits ($n \rightarrow \pi^*$) transition character. In contrast, in isolated uracil, the S_1 state is an ($n \rightarrow \pi^*$) state, and the states S_2−S_4 are ($\pi \rightarrow \pi^*$) states. For this system, the molecular orbital picture is insufficient to analyze the character of the excited states properly because many orbital transitions contribute to the excitation, and the orbitals themselves change both in form and energetic order

Table 2. Excitation Energies, Oscillator Strengths, and Main Orbital Transitions (>10%) for the Five Energetically Lowest Electronically Excited Singlet States[a] of Isolated Benzaldehyde and $[BA{\cdot}2H_2O]$ Using Supermolecular ADC(3) and FDE-ADC(3) with the RADM Approximation

	excitation energies [eV] and osc. str.			orb. trans.	weight [%]		
state[a]	iso.[b]	sup.[c]	FDE[d]	H + x → L + y[e]	iso.[b]	sup.[c]	FDE[d]
S_1	3.827 (0.0002)	4.063 (0.0003)	4.038 (0.0002)	−2 → 3 ($n \rightarrow \pi^*$)	63.4[f]	63.5	65.5
S_2	4.554 (0.0110)	4.454 (0.0188)	4.476 (0.0157)	0 → 3 ($\pi \rightarrow \pi^*$)	19.0[f,g]	53.1[g]	52.0
				−1 → 3 ($\pi \rightarrow \pi^*$)	36.2[f,g]	5.2[g]	7.6
				−1 → 8 ($\pi \rightarrow \pi^*$)			12.9
S_3	5.334 (0.2827)	5.160 (0.2878)	5.207 (0.3006)	−1 → 3 ($\pi \rightarrow \pi^*$)	24.0[f,g]	66.3[g]	66.0
				0 → 3 ($\pi \rightarrow \pi^*$)	54.0[f,g]	8.7[g]	12.1
S_5	6.476 (0.3487)	6.368 (0.3084)	6.399 (0.2874)	0 → 8 ($\pi \rightarrow \pi^*$)	19.3[g]		6.1[h]
				0 → 3 ($\pi \rightarrow \pi^*$)		16.5[g]	17.1[h]
				−1 → 3 ($\pi \rightarrow \pi^*$)	19.0[g,f]		4.5[h]
				0 → 7 ($\pi \rightarrow \pi^*$)	13.8[g,h]		
				−1 → 8 ($\pi \rightarrow \pi^*$)	10.0[g,h]	13.8[g,h]	36.7[h]
				−1 → 12 ($\pi \rightarrow \pi^*$)		13.5[g,h]	

[a]Note that the S_4 state did not converge in all calculations. [b]Isolated benzaldehyde. [c]Supersystem ADC(3) calculation. [d]RADM-FDE-ADC(3). [e]H = HOMO, L = LUMO. [f]A Rydberg orbital is neglected in counting, i.e., LUMO indices reduced by 1 to match the numbers. [g]Because HOMO and HOMO−1 are differently oriented in [b]iso. and [c]sup., the energetic numbering might not necessarily match. [h]Because various Rydberg orbitals change their energetic ordering, orbital indices might not match.

DOI: 10.1021/acs.jctc.7b00461
J. Chem. Theory Comput. 2017, 13, 4711−4725

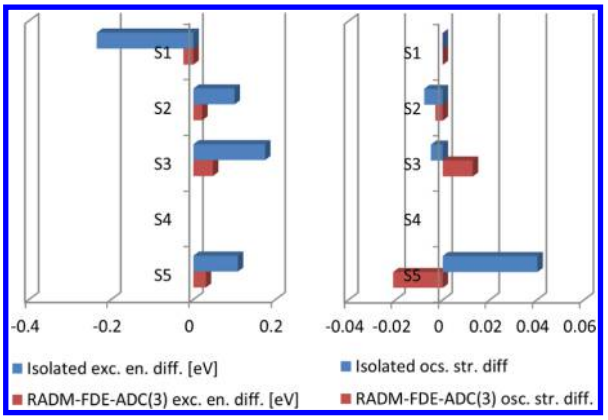

Figure 6. Analysis of the accuracy of FDE-ADC(3) of [BA·2H_2O]. Excitation energy difference (left) and oscillator strength difference (right) of the isolated benzaldehyde to the supersystem (blue) and the FDE-ADC(3) calculation using the RADM approximation to the supersystem (red). The blue bars correspond to the solvatochromic shift, whereas the red bars indicate the accuracy of the FDE-ADC(3) calculation in comparison with the supermolecular ADC(3) calculation.

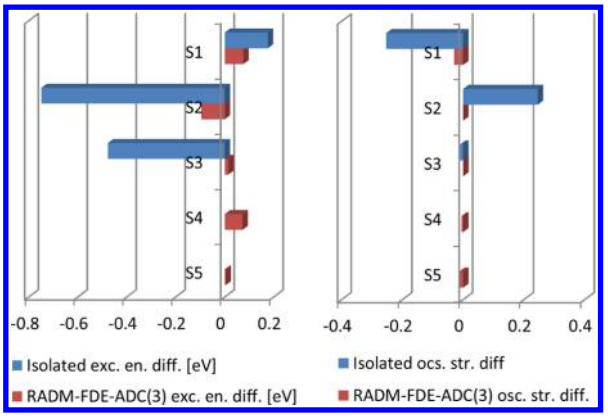

Figure 7. Analysis of the accuracy of FDE-ADC(3) for [UC·5H_2O]. Excitation energy difference (left) and oscillator strength difference (right) of the isolated uracil to the supersystem (blue) and the FDE-ADC(3) calculations using the RADM approximation to the supersystem (red). The blue bars correspond to the solvatochromic shift, and the red bars indicate the accuracy of the FDE-ADC(3) calculation in comparison to the supermolecular ADC(3) calculation. The results for states S_4 and S_5 of isolated uracil are excluded.

between isolated uracil and [UC·5H_2O]. Therefore, natural transition orbitals (NTOs)[76−78] have been calculated and analyzed to characterize the excited states. These NTOs reveal the S_1 state of isolated uracil to correspond to the S_2 state of [UC·5H_2O], whereas the S_1 state of the supersystem corresponds to the S_2 state of isolated uracil. The S_3 state is identical in both cases, and the S_4 and S_5 states in [UC·5H_2O] exhibit different character than any of the calculated states of isolated uracil. These states are energetically lowered by the environment. An electronic state of [UC·5H_2O] corresponding to the S_4 state of isolated uracil could not be identified. To facilitate comparison of corresponding states, each state is assigned to a Greek letter based on its character and not on its energetic order (see Table 3).

In the FDE-ADC(3) calculation, the effect of the environment on the embedded system is generally well reproduced. HOMO and HOMO−1 exhibit π character, HOMO−2 and HOMO−3 show n character, and each is localized on one oxygen atom. The excited states have the same character and energetic order as in the supermolecular calculation. With an MAE of 0.053 eV for excitation energies and 0.01 for oscillator strengths, the excited state properties are also in good agreement with the supermolecular calculation. This is displayed in Figure 7. However, because the S_5 state did not converge in the isolated uracil calculation and the S_4 state differs from the S_4 state in the supermolecular calculations, these values are excluded from the comparison. Additionally, because the energetic order of the states changes from isolated uracil to [UC·5H_2O], the comparison is based on the character of the states and the assingment has been done according to the supermolecular results.

5. REPRESENTATIVE APPLICATIONS OF FDE-ADC

After benchmarking FDE-ADC(3) in the previous section, the potential of the FDE-ADC method shall be demonstrated at three representative examples, which comprise computations of larger systems. For these, supermolecular calculations at the ADC(3) level are no longer feasible, and instead, the RADM approximation has to be employed. In the first example, the excited states of benzoquinone solvated in methanol are investigated. In the second example, the photoswitch spiropyran dissolved in water is analyzed and compared to QM/MM calculations from the literature.[79] In the third example, the core-excited states of CO@C_{60}, a CO molecule caught in a C_{60} fullerene, are calculated using the core−valence-separated FDE-CVS-ADC method. The different influences of a C_{60} cage on the core excitations in carbon monoxide are investigated.

5.1. Excited States of *p*-Benzoquinone in Methanol. To simulate *p*-benzoquinone in methanol solution, a *p*-benzoquinone molecule was surrounded by 42 methanol molecules. Benzoquinone was chosen as an example because it is a symmetric molecule of moderate size, has a delocalized π-electron system, can act as hydrogen bond acceptor, and exhibits

Table 3. Excitation Energies and Oscillator Strengths for the Five Energetically Lowest Electronically Excited Singlet States of Isolated Uracil, [UC·5H_2O], at the Supermolecular ADC(3) Level as Well as at the FDE-ADC(3) Level with the RADM Approximation

	excitation energies [eV] and osc. str.			transition character		
state	iso.[a]	sup.[b]	FDE[c]	iso.[a]	sup.[b]	FDE[c]
S_1	5.015 (0.0000)	5.123 (0.2534)	5.199 (0.2235)	$(n \rightarrow \pi^*)(\alpha)$	$(\pi \rightarrow \pi^*)(\beta)$	$(\pi \rightarrow \pi^*)(\beta)$
S_2	5.299 (0.2454)	5.764 (0.0000)	5.668 (0.0000)	$(\pi \rightarrow \pi^*)(\beta)$	$(n \rightarrow \pi^*)(\alpha)$	$(n \rightarrow \pi^*)(\alpha)$
S_3	5.716 (0.0027)	6.193 (0.0130)	6.208 (0.0132)	$(\pi \rightarrow \pi^*)(\gamma)$	$(\pi \rightarrow \pi^*)(\gamma)$	$(\pi \rightarrow \pi^*)(\gamma)$
S_4	6.330 (0.0341)	6.383 (0.1014)	6.456 (0.0957)	$(\pi \rightarrow \pi^*)(\delta)$	$(\pi \rightarrow \pi^*)(\epsilon)$	$(\pi \rightarrow \pi^*)(\epsilon)$
S_5		6.627 (0.2207)	6.631 (0.2069)		$(\pi \rightarrow \pi^*)(\zeta)$	$(\pi \rightarrow \pi^*)(\zeta)$

[a]Isolated uracil. [b]Supermolecular ADC(3). [c]RADM-FDE-ADC(3).

DOI: 10.1021/acs.jctc.7b00461
J. Chem. Theory Comput. 2017, 13, 4711−4725

low-lying electronically excited states with both single and double excitation character. Therefore, a quantum chemical method including doubly excited configurations in more than zeroth order of perturbation theory, like ADC(3), is needed to describe the excitations properly.[32] Because benzoquinone is soluble in moderately polar solvents, methanol was chosen as the environment. The supersystem is shown in Figure 8.

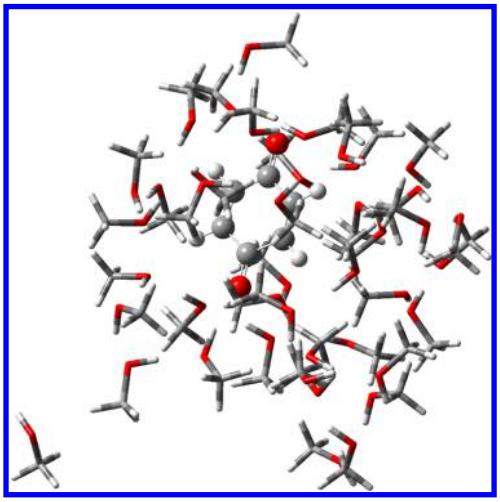

Figure 8. Supersystem of benzoquinone (balls and sticks, embedded system (A)) and 42 methanol molecules (environment (B)).

Isolated benzoquinone was optimized at the MP(2)/cc-pVTZ level of theory. This geometry serves as the reference for gas-phase calculations. Additionally, the supersystem of benzoquinone and 42 methanol molecules placed around the benzoquinone was fully optimized at the DFT/ωB97X-D3[80]/6-31G* level of theory. The initial structure was created manually and has been preoptimized using a generic force field. The optimized structure was used for investigating the effects of the environment. The obtained structure is just one possible representative simulating an environment, and for the purpose here, it is not necessary to be the energetically lowest possible structure. The two energetically lowest excited states of *p*-benzoquinone are investigated at the ADC(3)/6-311G** level of theory for the two isolated benzoquinone structures, i.e., one optimized at the MP(2) level in the gas phase and the other cut out of the methanol environment, and at the FDE-ADC(3)/6-311G** level of theory for the supersystem. For the FDE-ADC(3) calculation, the RADM approximation was used, the density of the environment was calculated at the HF level of theory, and the nonelectrostatic part of the embedding potential was calculated employing the PBE functional. In the gas phase, these states are with excitation energies of 2.840 and 2.999 eV close in energy. Both are ($n \rightarrow \pi^*$) states each containing transitions from both *n* orbitals localized at the oxygen atoms. Therefore, both excited states have no oscillator strength (both 0.000). The excitation character is visualized by attachment and detachment densities (Figure 9). The detachment density is the part of the total electron density that is removed upon excitation and replaced by the attachment density. In combination, they unambiguously characterize the electronic transition.

A very similar excitation pattern is obtained for the supersystem-optimized isolated benzoquinone structure. Both S_1 and S_2 exhibit ($n \rightarrow \pi^*$) transition character. Because the geometry is slightly different, the excitation energies also vary slightly and correspond to 2.893 and 3.077 eV for S_1 and S_2, respectively. The oscillator strengths of both states are still zero, and the attachment and detachment densities are practically identical to the gas-phase picture. However, they are slightly distorted due to the solvation-induced changes in the geometry (Figure S1).

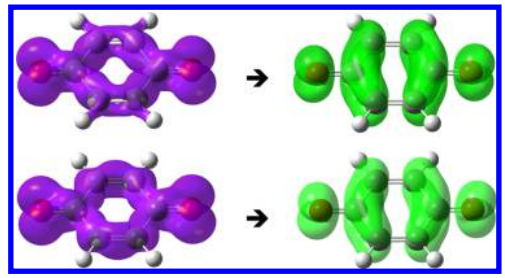

Figure 9. Detachment (left) and attachment (right) densities of the S_1 (top) and S_2 state of isolated gas-phase benzoquinone.

A different picture is obtained when the environment is included via FDE. Whereas the excitation energy of the first excited state is almost identical to the isolated calculation in the supersystem-optimized geometry, the excitation energy of the second excited state is increased by ~0.23 eV. Although both excited states are still ($n \rightarrow \pi^*$) states, they are now localized on one of the oxygen atoms each. The environment induces a separation and localization of the two excited states. This is nicely identified by the attachment and detachment densities (Figure 10).

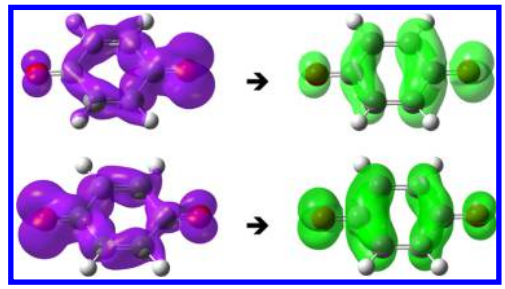

Figure 10. Detachment (left) and attachment (right) densities of the S_1 (top) and S_2 state (bottom) of benzoquinone embedded in 42 methanol molecules at the FDE-ADC(3) level of theory.

5.2. Transition Densities of Spiropyran in Water.

Spiropyran is a molecular photoswitch that undergoes a ring-opening and isomerization reaction upon irradiation with UV light.[81−83] The photoisomerization process has been investigated spectroscopically using femtosecond vis-pump/vis- and IR-probe spectroscopy,[84,85] and previous QM/MM calculations on spiropyran in water demonstrated only a small influence of water on the vertical excitations and photochemistry of spiropyran.[79] The energetically lowest excited states have been characterized as "bright" and "dark" states, indicating the difference in oscillator strengths. Occupying the bright state leads to a ring-opening reaction to merocyanine. These two important excited states could be identified in the presence of the water environment as well.[79] This finding shall here be verified using FDE-ADC.

A supersystem of spiroypran and 100 water molecules arranged in at least two solvation shells around spiropyran was created manually and fully optimized at the DFT/ωB97X-D3/6-31G* level of theory after a preoptimization using a force field.

DOI: 10.1021/acs.jctc.7b00461
J. Chem. Theory Comput. 2017, 13, 4711−4725

This structure is used for the calculation of vertical excitation energies of isolated spiropyran as well as of the embedded system using FDE-ADC.

The calculations of the excited states have been performed at the ADC(2)/cc-pVDZ and FDE-ADC(2)/cc-pVDZ levels of theory. For the FDE-ADC(2) calculation, the environment density was calculated using HF, and the nonelectrostatic part of the embedding potential was calculated using the PBE functional. The geometry of the supersystem is shown in Figure 11.

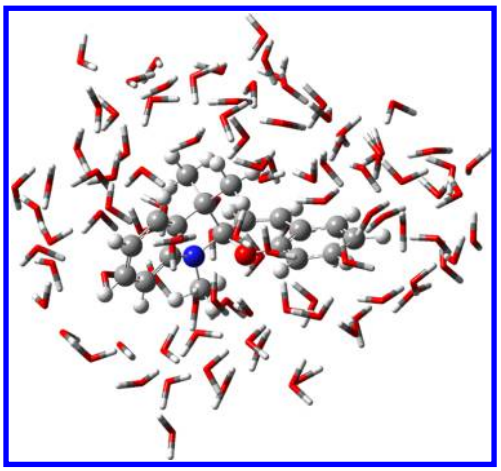

Figure 11. Supersystem of spiropyran (balls and sticks, embedded system (A)) surrounded by 100 water molecules (environment (B)).

The two energetically lowest excited states were calculated and analyzed using natural transition orbitals (NTOs).[76−78] NTOs are orbitals specific for one excitation and describe the electron transition itself. NTOs always come in pairs: one representing the particle and the other representing the hole. Both share the same eigenvalue, which corresponds to the contribution of this pair to the total excitation. Although it is mathematically not fully correct, for the sake of simplicity, the nomenclature used for molecular orbitals is also applied here. Therefore, the hole NTO exhibiting the highest eigenvalue is labeled "highest occupied natural transition orbital" (HONTO) and the corresponding particle NTO sharing the same eigenvalue is labeled "lowest unoccupied natural transition orbital" (LUNTO). The NTO pairs exhibiting lower eigenvalues follow the same scheme (HONTO−1, LUNTO+1, ...).

In isolated spiropyran, the S_1 and S_2 states exhibit excitation energies and oscillator strengths of 4.172 eV (0.0506) and 4.434 eV (0.0084), respectively. Analyzing the corresponding NTOs, the S_1 state can be identified as local ($\pi \rightarrow \pi^*$) transition on the benzopyran moiety and the S_2 state as a charge-transfer state from the indoline moiety to the benzopyran side. The leading NTO pairs for both the S_1 and S_2 states are shown in the Supporting Information. They are qualitatively identical to the NTOs shown in Figure 12.

In the FDE-ADC(2) calculation, the excitation energy of the S_1 state is increased, whereas the excitation energy of the S_2 state is decreased. The excitation energies and oscillator strengths of S_1 and S_2 are now 4.222 eV (0.0438) and 4.265 eV (0.0096), respectively; however, their transition character is not changed compared to that of isolated spiropyran. The leading NTO pairs of the two energetically lowest excited states are given in Figure 12.

These results confirm previous studies of spiropyran in water on the QM/MM level of theory.[79] The water environment shifts

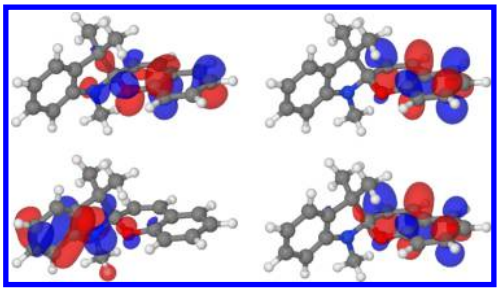

Figure 12. HONTO (left) and LUNTO (right) of the S_1 (top) and S_2 (bottom) states of spiropyran calculated with FDE-ADC(2).

the vertical excitation energies slightly but does not affect the photochemistry of spiropyran significantly, it still functions as a photoswitch in water.

5.3. Core Excited States of Carbon Monoxide in Fullerene. For the computation of core-excited states, the core−valence separation can be employed within ADC schemes, and an efficient computer program has recently been developed.[47−50] This dramatically facilitates the calculation of energetically high lying core-excited states.

In this section, the influence of a C_{60} cage on the core excitations of a carbon monoxide incorporated in C_{60} are demonstrated. For that purpose, CO@C_{60} was created and fully optimized at the DFT/ωB97X-D3/6-31G* level of theory. The system is shown in Figure 13.

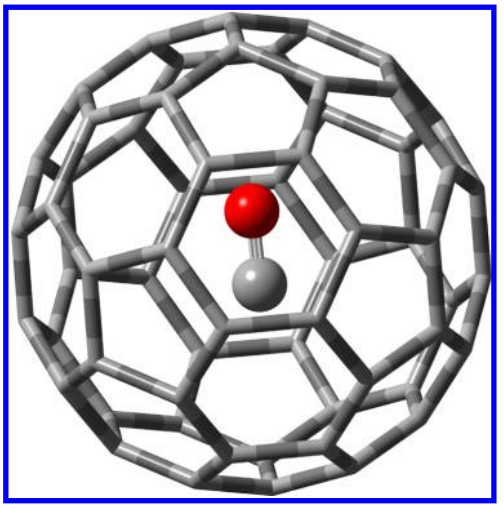

Figure 13. CO@C_{60} drawn as balls and sticks (embedded system (A)) and C_{60} molecule (environment (B)).

For comparison, the five energetically lowest (C_{1s}) core-excited states were calculated at the CVS-ADC(2)-x/6-311++G** level of theory for isolated CO. The core-excited states S_1^c−S_5^c exhibit the following character: ($C_{1s} \rightarrow \pi^*$), ($C_{1s} \rightarrow \pi^*$), ($C_{1s} \rightarrow \sigma^*$), ($C_{1s} \rightarrow \pi^*$), and ($C_{1s} \rightarrow \pi^*$), respectively. The corresponding excitation energies are given in Table 4. S_1^c and S_2^c as well as S_4^c and S_5^c are degenerate.

Employing the FDE-ADC approach for including the effect of C_{60}, the five energetically lowest core excited states were recalculated including the embedding potential obtained from an HF calculation for the electron density of C_{60} and the PBE functional for the nonelectrostatic part of $v_{emb}^{lin}(\vec{r})$ using the RADM approximation. Including the environment in the calculation of core excited states via FDE-CVS-ADC shows

DOI: 10.1021/acs.jctc.7b00461
J. Chem. Theory Comput. 2017, 13, 4711−4725

Table 4. Excitation Energies and Oscillator Strengths of the Five Energetically Lowest C_{1s} Core Excitations of Isolated CO and CO@C_{60} Using the FDE-CVS-ADC(2)-x Method

	core-excited states C_{1s}	
state	iso. CVS-ADC(2)-x	FDE-CVS-ADC(2)-x
S_1	287.730 (0.071)	287.656 (0.073)
S_2	287.730 (0.071)	287.659 (0.073)
S_3	293.299 (0.004)	293.493 (0.003)
S_4	294.577 (0.010)	294.593 (0.006)
S_5	294.577 (0.010)	294.628 (0.007)

only small influences. All calculated C_{1s} core-excited states are very similar to the results obtained for isolated CO regarding energies as well as properties and characters. This is verified by difference density analysis. The largest energetic shift is observed for the S_3^c state with ~0.2 eV. The excitation character of all five calculated states is retained. However, because C_{60} breaks the symmetry of CO, S_1^c and S_2^c as well as S_4^c and S_5^c are not fully degenerate any more. In Table 4, the excitation energies and oscillator strengths for the five energetically lowest C_{1s} core excitations are given.

The difference density plots for the core-excited states of CO@C_{60} obtained using the FDE-CVS-ADC method are qualitatively identical to the ones obtained for isolated CO. Note that in the core-excited difference density plots most of the change in electron density is due to orbital relaxation effects.[50] The difference densities for the five energetically lowest C_{1s} core-excited states S_1^c to S_5^c obtained using FDE-CVS-ADC(2)-x are shown in Figure 14.

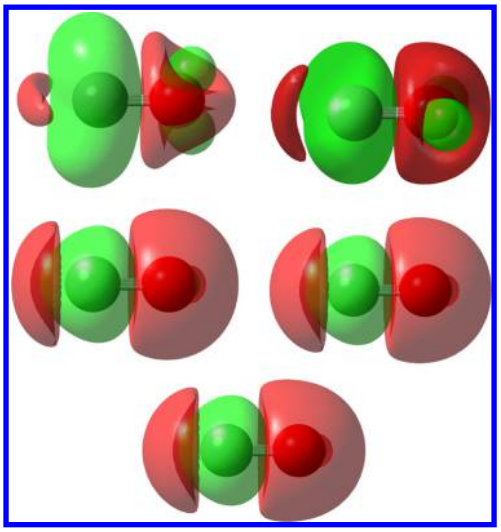

Figure 14. C_{1s} core-excited difference density plots of S_1^c (top left), S_2^c (top right), S_3^c (middle left), S_4^c (middle right), and S_5^c (bottom) of CO@C_{60} calculated using FDE-CVS-ADC(2)-x. The difference density plots for isolated CO are practically identical.

6. SUMMARY AND CONCLUSIONS

In this article, the implementation and application of the FDE-ADC approach up to third order of perturbation theory based on the combination of linearized FDET and ADC is presented. A previously published interface-based approach using both Molcas and Q-Chem[34] has been improved to a user-friendly Q-Chem-only implementation. Beyond a more straightforward application of FDE-ADC in general, this also enables the use of additional features already contained in the `adcman` module, for example, the core−valence separation (CVS) and wave function analysis tools (WFA). The implementation comprises now all available levels of ADC up to third order. The embedding scheme can be carried out in two different molecular orbital expansions. The supermolecular expansion expresses the embedding potential in the basis of both embedded system and environment and is only intended for benchmarking purposes of FDE-ADC. For productive calculations, the RADM approach is available in which the embedding potential is expressed only in the basis of the embedded system.

In the first tests and benchmarks, the choice of method used to calculate the environment density ρ_B using HF and DFT with various functionals and the choice of functional used to calculate the nonelectrostatic part of the embedding potential was evaluated. For this purpose, three benchmark systems have been employed: (1) benzene with one hydrogen fluoride molecule [BZ·HF], (2) benzaldehyde with a hydrogen-bonded water dimer [BA·2H_2O], and (3) uracil with five hydrogen-bonded water molecules [UC·5H_2O]. In summary, almost no dependence of the results on the employed functional for the calculation of the embedding potential could be observed. For the choice of the method used to calculate the environment, it could be seen that HF performs best and that the MAE is reduced with increasing amount of HF exchange. It is possible this behavior is due to the better match of an HF-based density for the environment with the HF/MP2-based density of the embedded system.

The same test systems were used to benchmark the accuracy of the new FDE-ADC(3) method by comparison to supermolecular calculations at the ADC(3) level of theory. For the FDE-ADC(3) calculations, HF and the functional PBE were chosen for the calculation of the environment density and the nonelectrostatic interaction, respectively. In all cases, the five energetically lowest excited states were calculated. The MAEs for the three systems are 0.001 eV for excitation energies and 0.0001 for oscillator strength for [BZ·HF], 0.031 eV (EE) and 0.0093 (OS) for [BA·2H_2O], and 0.053 eV (EE) and 0.01 (OS) for [UC·5H_2O]. This demonstrates the accuracy of the introduced FDE-ADC(3) method for very weak dispersive system−environment interactions up to very strong interactions via multiple hydrogen bonds.

In the last section, three representative applications of FDE-ADC on larger systems are presented. The splitting of two nearly degenerate ($n \rightarrow \pi^*$) excited states of benzoquinone due to a methanol environment is analyzed. The influence of a water environment onto the excited states of the photoswitch spiropyran is investigated, and the influence of the C_{60} cage onto the C_{1s} core-excited states of CO in CO@C_{60} is computed using FDE-CVS-ADC. In all three cases, the specific excitation properties are visualized by transition and difference density analyses.

In a future extension of the FDE-ADC implementation, the so-called monomer expansion (ME) will be implemented. In this approach, each subsystem is calculated in its own molecular orbital basis only, and thus, the error introduced by the truncation of the embedding potential as done in RADM is omitted. Furthermore, we intend to combine FDET with other wave function-based methods like coupled cluster theory,[86] which is quite straightforward in our implementation of `FDEman`.

In summary, the presented FDE-ADC implementation gives access to include explicit environment influences on the

DOI: 10.1021/acs.jctc.7b00461
J. Chem. Theory Comput. 2017, 13, 4711−4725

excitation process. Exhibiting an error lower than the intrinsic error of the used ADC method[32] makes FDE-ADC a reliable "black box" method for embedded systems in extended environments.

■ ASSOCIATED CONTENT

Supporting Information

The Supporting Information is available free of charge on the ACS Publications website at DOI: 10.1021/acs.jctc.7b00461.

Detailed analysis of the influence of the method and functional on the embedding potential in the three test systems [BZ·HF], [BA·2H_2O], and [UC·5H_2O]; figure of detachment and attachment densities of the S_1 and S_2 states of supersystem-optimized isolated benzoquinone; and figure of HONTO and LUNTO of the S_1 and S_2 states of isolated spiropyran (PDF)

■ AUTHOR INFORMATION

Corresponding Authors

*E-mail: stefan.prager@iwr.uni-heidelberg.de.
*E-mail: dreuw@uni-heidelberg.de.

ORCID

Andreas Dreuw: 0000-0002-5862-5113

Notes

The authors declare no competing financial interest.

■ ACKNOWLEDGMENTS

This research was supported by grants from the Swiss National Science Foundation (No. 200021_152779). S.P. thanks the Heidelberg Graduate School "Mathematical and Computational Methods for the Sciences" (HGS MathComp) for financial support. S.P. and A.Z. thank Prof. Yihan Shao and Prof. John Herbert for scientific discussions.

■ REFERENCES

(1) Liptay, W. Electrochromism and Solvatochromism. *Angew. Chem., Int. Ed. Engl.* **1969**, *8*, 177−188.
(2) Tomasi, J.; Mennucci, B.; Cammi, R. Quantum Mechanical Continuum Solvation Models. *Chem. Rev.* **2005**, *105*, 2999−3094.
(3) Mewes, J.-M.; You, Z.-Q.; Wormit, M.; Kriesche, T.; Herbert, J. M.; Dreuw, A. *J. Phys. Chem. A* **2015**, *119*, 5446.
(4) Mennucci, B.; Tomasi, J.; Cammi, R.; Cheeseman, J. R.; Frisch, M. J.; Devlin, F. J.; Gabriel, S.; Stephens, P. J. Polarizable Continuum Model (PCM) Calculations of Solvent Effects on Optical Rotations of Chiral Molecules. *J. Phys. Chem. A* **2002**, *106*, 6102−6113.
(5) Klein, R. A.; Mennucci, B.; Tomasi, J. Ab Initio Calculations of 17O NMR-Chemical Shifts for Water. The Limits of PCM Theory and the Role of Hydrogen-Bond Geometry and Cooperativity. *J. Phys. Chem. A* **2004**, *108*, 5851−5863.
(6) Warshel, A.; Levitt, M. Theoretical studies of enzymic reactions: Dielectric, electrostatic and steric stabilization of the carbonium ion in the reaction of lysozyme. *J. Mol. Biol.* **1976**, *103*, 227−249.
(7) Wesolowski, T. A.; Warshel, A. Frozen Density Functional Approach for Ab Initio Calculations of Solvated Molecules. *J. Phys. Chem.* **1993**, *97*, 8050−8053.
(8) Govind, N.; Wang, Y. A.; da Silva, A. J. R.; Carter, E. A. Accurate ab initio energetics of extended systems via explicit correlation embedded in a density functional environment. *Chem. Phys. Lett.* **1998**, *295*, 129−134.
(9) Bendavid, L. I.; Carter, E. A. *Status in Calculating Electronic Excited States in Transition Metal Oxides from First Principles*; Springer, 2014; pp 1−52.
(10) Wesolowski, T. A.; Shedge, S.; Zhou, X. Frozen-Density Embedding Strategy for Multilevel Simulations of Electronic Structure. *Chem. Rev.* **2015**, *115*, 5891−5928.
(11) Wesolowski, T. A. Embedding a Multideterminantal Wave Function in an Orbital-Free Environment. *Phys. Rev. A: At., Mol., Opt. Phys.* **2008**, *77*, 012504.
(12) Hohenberg, P.; Kohn, W. Inhomogeneous Electron Gas. *Phys. Rev.* **1964**, *136*, B864−B871.
(13) Kohn, W.; Sham, L. J. Self-Consistent Equations Including Exchange and Correlation Effects. *Phys. Rev.* **1965**, *140*, A1133−A1138.
(14) Parr, R.; Yang, W. *Density-functional theory of atoms and molecules*; Oxford University Press, Clarendon Press: New York, Oxford, England, 1989.
(15) Govind, N.; Wang, Y. A.; Carter, E. A. Electronic-structure calculations by first-principles density-based embedding of explicitly correlated systems. *J. Chem. Phys.* **1999**, *110*, 7677.
(16) Aquilante, F.; Wesołowski, T. a. Self-consistency in frozen-density embedding theory based calculations. *J. Chem. Phys.* **2011**, *135*, 084120.
(17) Daday, C.; König, C.; Valsson, O.; Neugebauer, J.; Filippi, C. State-specific embedding potentials for excitation-energy calculations. *J. Chem. Theory Comput.* **2013**, *9*, 2355−2367.
(18) Daday, C.; König, C.; Neugebauer, J.; Filippi, C. Wavefunction in density functional theory embedding for excited states: which wavefunctions, which densities? *ChemPhysChem* **2014**, *15*, 3205−17.
(19) Höfener, S.; Severo Pereira Gomes, A.; Visscher, L. Molecular properties via a subsystem density functional theory formulation: A common framework for electronic embedding. *J. Chem. Phys.* **2012**, *136*, 044104.
(20) Höfener, S. Coupled-cluster frozen-density embedding using resolution of the identity methods. *J. Comput. Chem.* **2014**, *35*, 1716−1724.
(21) Höfener, S.; Visscher, L. Wave Function Frozen-Density Embedding: Coupled Excitations. *J. Chem. Theory Comput.* **2016**, *12*, 549−557.
(22) Heuser, J.; Höfener, S. Wave-function frozen-density embedding: Approximate analytical nuclear ground-state gradients. *J. Comput. Chem.* **2016**, *37*, 1092−1101.
(23) Laktionov, A.; Chemineau-Chalaye, E.; Wesolowski, T. A. Frozen-density embedding theory with average solvent charge densities from explicit atomistic simulations. *Phys. Chem. Chem. Phys.* **2016**, *18*, 21069−21078.
(24) Dulak, M.; Kamiński, J. W.; Wesolowski, T. A. Linearized orbital-free embedding potential in self-consistent calculations. *Int. J. Quantum Chem.* **2009**, *109*, 1886−1897.
(25) Dresselhaus, T.; Neugebauer, J.; Knecht, S.; Keller, S.; Ma, Y.; Reiher, M. Self-consistent embedding of density-matrix renormalization group wavefunctions in a density functional environment. *J. Chem. Phys.* **2015**, *142*, 044111.
(26) Wesolowski, T. A. Embedding Potentials for Excited States of Embedded Species. *J. Chem. Phys.* **2014**, *140*, 18A530.
(27) Zech, A.; Aquilante, F.; Wesolowski, T. A. Orthogonality of embedded wave functions for different states in frozen-density embedding theory. *J. Chem. Phys.* **2015**, *143*, 164106.
(28) Dreuw, A.; Weisman, J. L.; Head-Gordon, M. Long-range charge-transfer excited states in time-dependent density functional theory require non-local exchange. *J. Chem. Phys.* **2003**, *119*, 2943−2946.
(29) Dreuw, A.; Head-Gordon, M. Failure of Time-Dependent Density Functional Theory for Long-Range Charge-Transfer Excited States: The Zincbacteriochlorin-Bacteriochlorin and Bacteriochlorophyll-Spheroidene Complexes. *J. Am. Chem. Soc.* **2004**, *126*, 4007−4016.
(30) Laurent, A. D.; Jacquemin, D. TD-DFT benchmarks: A review. *Int. J. Quantum Chem.* **2013**, *113*, 2019−2039.
(31) Wormit, M.; Rehn, D. R.; Harbach, P. H.; Wenzel, J.; Krauter, C. M.; Epifanovsky, E.; Dreuw, A. Investigating excited electronic states using the algebraic diagrammatic construction (ADC) approach of the polarisation propagator. *Mol. Phys.* **2014**, *112*, 774−784.
(32) Harbach, P. H. P.; Wormit, M.; Dreuw, A. The third-order algebraic diagrammatic construction method (ADC(3)) for the

polarization propagator for closed-shell molecules: Effcient implementation and benchmarking). *J. Chem. Phys.* **2014**, *141*, 064113.
(33) Dreuw, A.; Wormit, M. The algebraic diagrammatic construction scheme for the polarization propagator for the calculation of excited states. *WIREs Comput. Mol. Sci.* **2015**, *5*, 82−95.
(34) Prager, S.; Zech, A.; Aquilante, F.; Dreuw, A.; Wesolowski, T. A. First time combination of frozen density embedding theory with the algebraic diagrammatic construction scheme for the polarization propagator of second order. *J. Chem. Phys.* **2016**, *144*, 204103.
(35) Schirmer, J. Beyond the random-phase approximation: A new approximation scheme for the polarization propagator. *Phys. Rev. A: At., Mol., Opt. Phys.* **1982**, *26*, 2395−2416.
(36) Trofimov, A. B.; Schirmer, J. An efficient polarization propagator approach to valence electron excitation spectra. *J. Phys. B: At., Mol. Opt. Phys.* **1995**, *28*, 2299.
(37) Mertins, F.; Schirmer, J. Algebraic propagator approaches and intermediate-state representations. I. The biorthogonal and unitary coupled-cluster methods. *Phys. Rev. A: At., Mol., Opt. Phys.* **1996**, *53*, 2140−2152.
(38) Schirmer, J.; Trofimov, A. B. Intermediate state representation approach to physical properties of electronically excited molecules. *J. Chem. Phys.* **2004**, *120*, 11449−11464.
(39) Trofimov, A. B.; Stelter, G.; Schirmer, J. A consistent third-order propagator method for electronic excitation. *J. Chem. Phys.* **1999**, *111*, 9982−9999.
(40) Neugebauer, J. Couplings between electronic transitions in a subsystem formulation of time-dependent density functional theory. *J. Chem. Phys.* **2007**, *126*, 134116.
(41) Aquilante, F.; Wesołowski, T. a. Self-consistency in frozen-density embedding theory based calculations. *J. Chem. Phys.* **2011**, *135*, 084120.
(42) Shao, Y.; Gan, Z.; Epifanovsky, E.; Gilbert, A. T.; Wormit, M.; Kussmann, J.; Lange, A. W.; Behn, A.; Deng, J.; Feng, X.; Ghosh, D.; Goldey, M.; Horn, P. R.; Jacobson, L. D.; Kaliman, I.; Khaliullin, R. Z.; Kuś, T.; Landau, A.; Liu, J.; Proynov, E. I.; Rhee, Y. M.; Richard, R. M.; Rohrdanz, M. A.; Steele, R. P.; Sundstrom, E. J.; Woodcock, H. L., III; Zimmerman, P. M.; Zuev, D.; Albrecht, B.; Alguire, E.; Austin, B.; Beran, G. J. O.; Bernard, Y. A.; Berquist, E.; Brandhorst, K.; Bravaya, K. B.; Brown, S. T.; Casanova, D.; Chang, C.-M.; Chen, Y.; Chien, S. H.; Closser, K. D.; Crittenden, D. L.; Diedenhofen, M.; DiStasio, R. A., Jr.; Do, H.; Dutoi, A. D.; Edgar, R. G.; Fatehi, S.; Fusti-Molnar, L.; Ghysels, A.; Golubeva-Zadorozhnaya, A.; Gomes, J.; Hanson-Heine, M. W.; Harbach, P. H.; Hauser, A. W.; Hohenstein, E. G.; Holden, Z. C.; Jagau, T.-C.; Ji, H.; Kaduk, B.; Khistyaev, K.; Kim, J.; Kim, J.; King, R. A.; Klunzinger, P.; Kosenkov, D.; Kowalczyk, T.; Krauter, C. M.; Lao, K. U.; Laurent, A. D.; Lawler, K. V.; Levchenko, S. V.; Lin, C. Y.; Liu, F.; Livshits, E.; Lochan, R. C.; Luenser, A.; Manohar, P.; Manzer, S. F.; Mao, S.-P.; Mardirossian, N.; Marenich, A. V.; Maurer, S. A.; Mayhall, N. J.; Neuscamman, E.; Oana, C. M.; Olivares-Amaya, R.; O'Neill, D. P.; Parkhill, J. A.; Perrine, T. M.; Peverati, R.; Prociuk, A.; Rehn, D. R.; Rosta, E.; Russ, N. J.; Sharada, S. M.; Sharma, S.; Small, D. W.; Sodt, A.; Stein, T.; Stück, D.; Su, Y.-C.; Thom, A. J.; Tsuchimochi, T.; Vanovschi, V.; Vogt, L.; Vydrov, O.; Wang, T.; Watson, M. A.; Wenzel, J.; White, A.; Williams, C. F.; Yang, J.; Yeganeh, S.; Yost, S. R.; You, Z.-Q.; Zhang, I. Y.; Zhang, X.; Zhao, Y.; Brooks, B. R.; Chan, G. K.; Chipman, D. M.; Cramer, C. J.; Goddard, W. A., III; Gordon, M. S.; Hehre, W. J.; Klamt, A.; Schaefer, H. F., III; Schmidt, M. W.; Sherrill, C. D.; Truhlar, D. G.; Warshel, A.; Xu, X.; Aspuru-Guzik, A.; Baer, R.; Bell, A. T.; Besley, N. A.; Chai, J.-D.; Dreuw, A.; Dunietz, B. D.; Furlani, T. R.; Gwaltney, S. R.; Hsu, C.-P.; Jung, Y.; Kong, J.; Lambrecht, D. S.; Liang, W.; Ochsenfeld, C.; Rassolov, V. A.; Slipchenko, L. V.; Subotnik, J. E.; Van Voorhis, T.; Herbert, J. M.; Krylov, A. I.; Gill, P. M.; Head-Gordon, M. Advances in molecular quantum chemistry contained in the Q-Chem 4 program package. *Mol. Phys.* **2015**, *113*, 184−215.
(43) Cramer, C. *Essentials of computational chemistry: theories and models*; Wiley: Chichester, West Sussex, England; Hoboken, NJ, 2004.
(44) Jensen, F. *Introduction to computational chemistry*; John Wiley & Sons: Chichester, England; Hoboken, NJ, 2007.
(45) Szabo, A. *Modern quantum chemistry: introduction to advanced electronic structure theory*; Dover Publications: Mineola, NY, 1996.
(46) Gill, P. M.; Johnson, B. G.; Pople, J. A. A standard grid for density functional calculations. *Chem. Phys. Lett.* **1993**, *209*, 506−512.
(47) Wenzel, J.; Wormit, M.; Dreuw, A. Calculating core-level excitations and x-ray absorption spectra of medium-sized closed-shell molecules with the algebraic-diagrammatic construction scheme for the polarization propagator. *J. Comput. Chem.* **2014**, *35*, 1900−1915.
(48) Wenzel, J.; Wormit, M.; Dreuw, A. Calculating X-ray Absorption Spectra of Open- Shell Molecules with the Unrestricted Algebraic-Diagrammatic Construction Scheme for the Polarization Propagator. *J. Chem. Theory Comput.* **2014**, *10*, 4583−4598.
(49) Wenzel, J.; Holzer, A.; Wormit, M.; Dreuw, A. Analysis and comparison of CVS-ADC approaches up to third order for the calculation of core-excited states. *J. Chem. Phys.* **2015**, *142*, 214104.
(50) Wenzel, J.; Dreuw, A. Physical Properties, Exciton Analysis, and Visualization of Core-Excited States: An Intermediate State Representation Approach. *J. Chem. Theory Comput.* **2016**, *12*, 1314−1330.
(51) Plasser, F.; Wormit, M.; Dreuw, A. New tools for the systematic analysis and visualization of electronic excitations. I. Formalism. *J. Chem. Phys.* **2014**, *141*, 024106.
(52) Plasser, F.; Baeppler, S. A.; Wormit, M.; Dreuw, A. New tools for the systematic analysis and visualization of electronic excitations. II. Applications. *J. Chem. Phys.* **2014**, *141*, 024107.
(53) Plasser, F.; Thomitzni, B.; Bäppler, S. A.; Wenzel, J.; Rehn, D. R.; Wormit, M.; Dreuw, A. Statistical analysis of electronic excitation processes: Spatial location, compactness, charge transfer, and electron-hole correlation. *J. Comput. Chem.* **2015**, *36*, 1609−1620.
(54) Krauter, C. M.; Schimmelpfennig, B.; Pernpointner, M.; Dreuw, A. Algebraic diagrammatic construction for the polarization propagator with spin-orbit coupling. *Chem. Phys.* **2017**, *482*, 286−293. Electrons and nuclei in motion−correlation and dynamics in molecules (on the occasion of the 70th birthday of Lorenz S. Cederbaum).
(55) Hanwell, M.; Curtis, D.; Lonie, D.; Vandermeersch, T.; Zurek, E.; Hutchison, G. Avogadro: an advanced semantic chemical editor, visualization, and analysis platform. *J. Cheminf.* **2012**, *4*, 17.
(56) Persistence of Vision Raytracer Pty. Ltd, POV-Ray 3.7.
(57) Willighagen, E.; Howard, M. Fast and Scriptable Molecular Graphics in Web Browsers without Java3D. *Nature Precedings* **2007**, 1.
(58) Dennington, R.; Keith, T.; Millam, J. *GaussView*, version 5; Semichem Inc.: Shawnee Mission, KS, 2009.
(59) Becke, A. D. Density functional calculations of molecular bond energies. *J. Chem. Phys.* **1986**, *84*, 4524−4529.
(60) Lee, C.; Yang, W.; Parr, R. G. Development of the Colle-Salvetti correlation-energy formula into a functional of the electron density. *Phys. Rev. B: Condens. Matter Mater. Phys.* **1988**, *37*, 785−789.
(61) Perdew, J. P.; Burke, K.; Ernzerhof, M. Generalized Gradient Approximation Made Simple. *Phys. Rev. Lett.* **1996**, *77*, 3865−3868.
(62) Perdew, J. P. Density-functional approximation for the correlation energy of the inhomogeneous electron gas. *Phys. Rev. B: Condens. Matter Mater. Phys.* **1986**, *33*, 8822−8824.
(63) Perdew, J. P.; Chevary, J. A.; Vosko, S. H.; Jackson, K. A.; Pederson, M. R.; Singh, D. J.; Fiolhais, C. Atoms, molecules, solids, and surfaces: Applications of the generalized gradient approximation for exchange and correlation. *Phys. Rev. B: Condens. Matter Mater. Phys.* **1992**, *46*, 6671−6687.
(64) Becke, A. D. Density−functional thermochemistry. III. The role of exact exchange. *J. Chem. Phys.* **1993**, *98*, 5648−5652.
(65) Shao, Y.; Head-Gordon, M.; Krylov, A. I. The spin-flip approach within time-dependent density functional theory: Theory and applications to diradicals. *J. Chem. Phys.* **2003**, *118*, 4807−4818.
(66) Adamo, C.; Barone, V. Toward reliable density functional methods without adjustable parameters: The PBE0 model. *J. Chem. Phys.* **1999**, *110*, 6158−6170.
(67) Peverati, R.; Truhlar, D. G. Communication: A global hybrid generalized gradient approximation to the exchange-correlation functional that satisfies the second-order density-gradient constraint and has broad applicability in chemistry. *J. Chem. Phys.* **2011**, *135*, 191102.
(68) Gill, P. M. W. A new gradient-corrected exchange functional. *Mol. Phys.* **1996**, *89*, 433−445.

DOI: 10.1021/acs.jctc.7b00461
J. Chem. Theory Comput. 2017, 13, 4711−4725

(69) Yu, H. S.; Zhang, W.; Verma, P.; He, X.; Truhlar, D. G. Nonseparable exchange-correlation functional for molecules, including homogeneous catalysis involving transition metals. *Phys. Chem. Chem. Phys.* **2015**, *17*, 12146−12160.
(70) Peverati, R.; Zhao, Y.; Truhlar, D. G. Generalized Gradient Approximation That Recovers the Second-Order Density-Gradient Expansion with Optimized Across-the-Board Performance. *J. Phys. Chem. Lett.* **2011**, *2*, 1991−1997.
(71) Lundqvist, S., March, N. H., Eds. *Theory of the inhomogeneous electron gas*; Physics of solids and liquids; Plenum Press: New York and London, 1983.
(72) Dunning, T. H. Gaussian basis sets for use in correlated molecular calculations. I. The atoms boron through neon and hydrogen. *J. Chem. Phys.* **1989**, *90*, 1007−1023.
(73) Ditchfield, R.; Hehre, W. J.; Pople, J. A. Self−Consistent Molecular−Orbital Methods. IX. An Extended Gaussian−Type Basis for Molecular−Orbital Studies of Organic Molecules. *J. Chem. Phys.* **1971**, *54*, 724−728.
(74) Hehre, W. J.; Ditchfield, R.; Pople, J. A. Self−Consistent Molecular Orbital Methods. XII. Further Extensions of Gaussian−Type Basis Sets for Use in Molecular Orbital Studies of Organic Molecules. *J. Chem. Phys.* **1972**, *56*, 2257−2261.
(75) Hariharan, P. C.; Pople, J. A. The influence of polarization functions on molecular orbital hydrogenation energies. *Theoretica Chimica Acta* **1973**, *28*, 213−222.
(76) Luzanov, A. V.; Sukhorukov, A. A.; Umanskii, V. Application of transition density matrix for analysis of excited states. *Theor. Exp. Chem.* **1976**, *10*, 354−361.
(77) Martin, R. L. Natural transition orbitals. *J. Chem. Phys.* **2003**, *118*, 4775−4777.
(78) Mayer, I. Using singular value decomposition for a compact presentation and improved interpretation of the CIS wave functions. *Chem. Phys. Lett.* **2007**, *437*, 284−286.
(79) Prager, S.; Burghardt, I.; Dreuw, A. Ultrafast C Spiro -O Dissociation via a Conical Intersection Drives Spiropyran to Merocyanine Photoswitching. *J. Phys. Chem. A* **2014**, *118*, 1339−1349.
(80) Lin, Y.-S.; Li, G.-D.; Mao, S.-P.; Chai, J.-D. Long-Range Corrected Hybrid Density Functionals with Improved Dispersion Corrections. *J. Chem. Theory Comput.* **2013**, *9*, 263−272.
(81) Krysanov, S.; Alfimov, M. Ultrafast formation of transients in spiropyran photochromism. *Chem. Phys. Lett.* **1982**, *91*, 77−80.
(82) Ernsting, N. P. Transient optical absorption spectroscopy of the photochemical spiropyran-merocyanine conversion. *Chem. Phys. Lett.* **1989**, *159*, 526−531.
(83) Ernsting, N. P.; Dick, B.; Arthen-Engeland, T. The primary photochemical reaction step of unsubstituted indolino-spiropyrans. *Pure Appl. Chem.* **1990**, *62*, 1.
(84) Kohl-Landgraf, J.; Braun, M.; Özçoban, C.; Gonçalves, D. P. N.; Heckel, A.; Wachtveitl, J. Ultrafast Dynamics of a Spiropyran in Water. *J. Am. Chem. Soc.* **2012**, *134*, 14070−14077.
(85) Kohl-Landgraf, J.; Braun, M.; Özçoban, C.; Goncalves, D.; Heckel, A.; Wachtveitl, J.; Chergui, M.; Taylor, A.; Cundiff, S.; Vivie-Riedle, R. d.; Yamagouchi, K. Dynamics of a photochromic spiropyran under aqueous conditions. *EPJ Web Conf.* **2013**, *41*, 05009.
(86) Helgaker, T.; Olsen, J.; Jørgensen, P. *Molecular Electronic-Structure Theory*; Wiley-Blackwell: Chichester, England, 2013.

DOI: 10.1021/acs.jctc.7b00461
J. Chem. Theory Comput. 2017, 13, 4711−4725